International Research Journal of Engineering and Technology (IRJET) e-ISSN: 2395-0056
Volume: 07 Issue: 04 | Apr 2020 www.irjet.net p-ISSN: 2395-0072

Design and Optimization Based on Surrogate Model of a Brushless Direct Current Motor for Light Electrical Vehicle

Almarri Jaber[1‡] , Esmail Elhomdy [2‡], Zheng Liu[1], and Guofeng Li [1*]

[1] School of Electrical Engineering, Dalian University of Technology, Dalian 116023, China
[2]Faculty of Engineering, Blue Nile University, Blue Nile State, 26613, Sudan;

Abstract – *This paper presents a brushless direct current motor (BLDCM) that is optimized based on surrogate models (SMs). It is aimed to achieve high efficiency under the most operated load conditions for light electric vehicle application. Designs of experiment (DOE) techniques are used, whilst one of these, the Latin hypercube sampling (LHS), is selected to generate the random and uniform sampling distributions. A sensitivity analysis (SA) is carried out to identify the important independent design variables (IDVs). The number of IDVs is reduced from 9 to 7 based on SA. The SMs of the BLDCM performance are constructed by using LHS and the Kriging modeling. The particle swarm optimization (PSO) based SMs techniques is adopted to optimize the BLDCM. The optimized results are successfully validated by using the finite element analysis (FEA). The computational cost of the proposed technique of optimizations based on SMs is lower than the conventional optimal design techniques based on an FEA. The BLDCM is evaluated in 2D FEA software.*

Key Words: **finite element analysis, multi-objective optimization, particle swarm optimization, sensitivity analysis, surrogate model, brushless direct current motor.**

1.INTRODUCTION

With energy crisis and environmental pollution becoming more prominent, hybrid electrical vehicles (HEVs) and electrical vehicles (EVs) as two effective solutions have been paid comprehensive attention by researchers. Motor and drive system are core component and common key technologies for EVs. Because of the advantages of high torque density, high efficiency and wide speed range, the brushless direct current motor (BLDCM) has been used in commercial HEVs successfully [1,2]. This research study aims to design and optimize an in-wheel motor that can maximize efficiency, as well as reduce the torque ripple and cogging torque.

An optimized processor is generally combined with an FEA simulation for the electrical machine design optimization (EMDO), which has higher calculation time, particularly for multi-objective (MO) optimization issues. Overall, a new optimization solution is required. Surrogate models (SMs) based on the design of experiment (DoE) and stochastic evolutionary methods are two methods utilized for the electrical machine design optimization [3,4]. The Latin hypercube sampling (LHS) and central composite design (CCD) method are types of DoE. The element samples are only dispersed at the center and corner of the design space in the CCD, this disadvantage makes it complicated to accurately assemble the overall apparatus performance information on extended design space. The LHS is a random sampling technique that has the advantages of flexibility and an ideal space filling feature [5]. The number of generation samples of the LHS can be controllable. The SMs methodology is a helpful tool for the analysis and optimization of computationally expensive models [6-8]. It provides a compromise between the high-precision low-speed calculations finite-element analysis (FEA) and high-speed low-accuracy simplified analytical methods. An SM is constructed by using the data obtained from an FEA, and it gives quick approximations of constraints and objectives at new design points so that optimization studies are practicable [9]. SMs have recently been used in machine design [10,11]. Stochastic evolutionary methods (SEMs), which are as PSO and genetic algorithm (GA) [12], are appropriate in EMDO. However, they are searching a high dimension of the design space in computation efficient technique [13].

The SEMs have been combined with an FEA in order to optimize the performances of BLDCM that has a high time of computational cost [14, 15]. The EMDO processes integrate SEMs and SMs to minimize the computational cost. The optimization of BLDCM based on surrogate optimization is investigated in this paper.

2. Design of an Out-Rotor BLDCM for the Light Electric Vehicle

The design of an out-rotor BLDC motor for the light electric vehicle is carried-out. In this paper, the wheel motor parameters are determined by analyzing the dynamic model of the electric vehicle and its actual operating conditions. Based on the analysis of the electric vehicle parameters [16,17], the parameters of the proposed electric vehicle are specified in Table 1.

Table -1 The parameters of the proposed electric vehicle

Parameter	Symbol	Value
The entire vehicle mass (kg)	M	600
Maximum speed (km/h)	μ_{max}	60
Rate speed (km/h)	μ_n	30
Windward area (m^2)	A_S	2
Coefficient of air resistance	C_d	0.4
Rolling resistance coefficient	f	0.015
Tyre size		145/60R13
Maximum climbing degree (deg)	α	11.3
0–50 km/h acceleration time (s)	t_a	9
System transmission efficiency	η_T	0.95

2.1. Design Requirements for Drive Motor Performance

The power of the motor must be able to meet the requirements of the motor drive in electric vehicle. The power calculation of the proposed motor can be estimated according to the different working conditions of the vehicle, such as working at maximum speed, climbing and accelerating [18,19].

The power of the motor to the vehicle working in the maximum speed, μ_{max} can be obtained as

$$P_a = \frac{\mu_{max}}{3600\eta_T}\left(mgf + \frac{A_s C_D \mu_{max}^2}{21.15}\right) \quad (1)$$

When the vehicle is climbing the power of the motor can be given by

$$P_b = \frac{\mu_i}{3600\eta_T}\left(mgf\cos\alpha + mg\sin\alpha + \frac{A_s C_D \mu_i^2}{21.15}\right) \quad (2)$$

The power of the motor for the accelerating vehicle can be presented as

$$P_c = \frac{\mu_a}{3600 t_a \eta_T}\left(m\delta\frac{\mu_a}{2\sqrt{t_a}} + mgf\frac{\mu_a}{1.5}t_a + \frac{A_s C_D \mu_a^2}{52.875}t_a\right) \quad (3)$$

where δ vehicle rotation mass conversion coefficient; m vehicle mass (kg); f rolling resistance coefficient; G gravity acceleration; α maximum climbing slope; μ_a acceleration end speed; μ_{max} maximum speed (km/ h); C_D air damping coefficient; t_a acceleration time (s); η_T transmission efficiency.

Then, from the above equation and Table 1, the power of the propose BLDCM is deduced as

$$P \geq \max[P_a, P_b, P_c] = [10.43, 7.35, 19.21]\ [\text{kW}]$$

Considering the three performance requirements of the electric vehicle, the peak power required by the vehicle is 19.21 kw. It is preliminarily determined that the peak power of the electric vehicle motor is 20kw, so the rated power of the single electric vehicle, P_N is 10 kW.

The design of the motor is based on the maximum speed of 60 km/h and rate speed 30 km/h as mentioned in Table 1. Therefore, the maximum speed, n_{max} of the motor can be given as:

$$n_{max} \geq \frac{\mu_{max} * 10^3}{120\pi r} \quad \text{rpm} \quad (4)$$

Tire specifications 145/60R13 is utilized, then the wheel radius can be about $r = 156.5$ mm.

From the above formula, the rated speed of the in-wheel motor, n_N is 500 rpm. The maximum speed is 850 rpm. The relationship between the rated torque of the motor, the rated speed, and the rated power are obtained as:

$$T_N = \frac{30P_N}{\pi n_N} \quad (5)$$

Thus, the rated torque of the motor, T_N is 190.98 Nm. Based on the above analysis, the design requirements of the drive motor are presented in Table 2.

Table-2 Design requirements for drive motor performance

Parameter	Value
Rated voltage (V)	72
Peak Power (kW)	15
Rated Power (kW)	10
Rated Torque (Nm)	190.98
Rated Speed (rpm)	500

2.2 Main Dimensions of the Motor

In order to develop the design, the geometrical configuration of the motor, phase number, stator, and rotor tooth numbers, and winding are considered. The main dimensions of the motor include the out diameter of the stator and the length of the stator core. The electromagnetic load includes the electrical load As and magnetic load Bδ of the motor, which are closely related to the main dimensions of the motor. These loads exert a significant influence on the mechanical characteristics, efficiency, torque, and other performance parameters of the motor. The relation between the main dimensions of the motor and the electromagnetic load is obtained as

$$D_{so}^2 L_a = \frac{6.1}{\alpha_m A_s B_\delta k_w k_{dq}} \frac{P_N}{n_N} \quad (6)$$

where k_w is the winding factor, k_{dq} is the waveform coefficient of the air gap magnetic field, D_{so} is the stator out diameter (mm), L_a is the length of the stator core (mm), α_m is the pole-arc coefficient is 0.75, A_s is the electrical load set to 25 A/mm in this study, and B_δ is the magnetic load set to be 0.96 T. Then, can be used Equation (6), in order to determine $D^2_a L_a$ as

$$D^2_a L_a = 7208 \times 10^3 \text{ mm}^3 \quad (7)$$

2.2.1 The Motor Configuration

There are many combinations of slots, poles, phases, and windings that lead to an acceptable motor design [19-21]. The primary constraint on the stator design is that the total number of stator slots can be some even integer multiple of the number of phases, i.e.

$$N_s = qN_{sp} \quad (8)$$

When N_{sp} is the even integer number of slots per phase and q is the number of phases, the number of slots per pole per phase is determined as

$$N_{spp} = \frac{N_s}{qN_m} = \frac{N_{sp}}{N_m} \quad (9)$$

When N_{spp} is fractional, cogging torque is reduced in addition to back emf smoothing [19-22]. Number of poles will be selected based on the speed of rotation, commutation frequency and cogging torque [20-21]. However, symmetrical phase flux-linkage and back-emf waveforms can be achieved by choosing an appropriate combination of stator and rotor pole numbers. Hence, in order to obtain symmetrical phase back-electromotive force (emf) waveforms, the number of stator poles and rotor poles must satisfy the Equation (10) [20-22].

$$\frac{N_s}{\gcd(N_s, N_r)} = \text{even number} \quad (10)$$

where *gcd* is the greatest common divisor

Thus, the relationship between the stator and rotor pole numbers for symmetrical and balanced back-emf waveforms can be obtained as:

$$\frac{N_s}{\gcd(N_s, N_m)} = 2qj \quad ,j = (1,2,3,\ldots) \quad (11)$$

Therefore, when the number of stator slot, N_s is 24, the combination of rotor poles, N_m of 4, 10 and 14 are exhibit symmetrical and balanced back-emf waveforms. Based on cogging torque reduction of BLDCM consists in a proper choice of the slot/pole number combination. The optimum choice for a minimum cogging torque should be done so as the greatest common divisor of N_s and N_m to be minimum [20-22]. Since the maximum torque is obtained when the Since the maximum torque is obtained when the rotor pole number is close to the stator pole number [23]. Based on the above equations (8), to (11), the configuration of BLDCM proposed in this paper has the number of stator slots, $N_s = 24$, and the number of rotor poles $N_m = 14$. This configuration has short end-windings and symmetrical back-emf waveforms [20-23]. Meanwhile, the construction of prototype 24/14 BLDCM is presented in Figure 1.

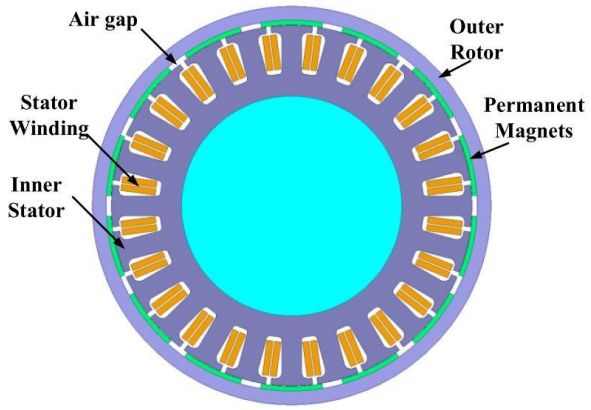

Figure-1 The construction of prototype 24/14 BLDCM

2.2.2 Dimensions of the Rotor

Based on a proposed vehicle, the tire specifications 145/60R13 is utilized, the outer diameter of the motor rotor, D_{ro} can be supposed as 313 mm. The mechanical integrity of the rotor and the operating flux density depend on the rotor yoke thickness, b_{ry}. It could have a value of the range satisfying the robust mechanics:

$$0.5\tau_s > b_{ry} \geq 0.2\tau_s \quad (12)$$

The pole pitch of the rotor given by: $\tau_r = \frac{\pi D_{ro}}{2N_r} = 35.11$ mm

Thereby, it is advised to choose a higher value, then the b_{ry} can be achieved by: $b_{ry} = 0.313\tau_r = 11$ mm

Due to the continuous innovation of permanent magnet material technology, there are more kinds of permanent magnet materials. Further, the performance of permanent magnet materials has been greatly improved. The main performance parameters of the permanent magnet chosen in this work are shown in Table 3.

Table-3 Characteristic parameters of NdFeB 42SH

Parameters	Value
Residual magnetic induction intensity, B_r (T)	1.28
Coercive fore, H_{cb} (kA/m)	939
Relative recovery permeability, μ_{rec}	1.085
Density, ρ_m (kg/m3)	7450

The working point of a permanent magnet is related to the energy of the motor. Figure 2 shows the B-H curve of a permanent magnet material.

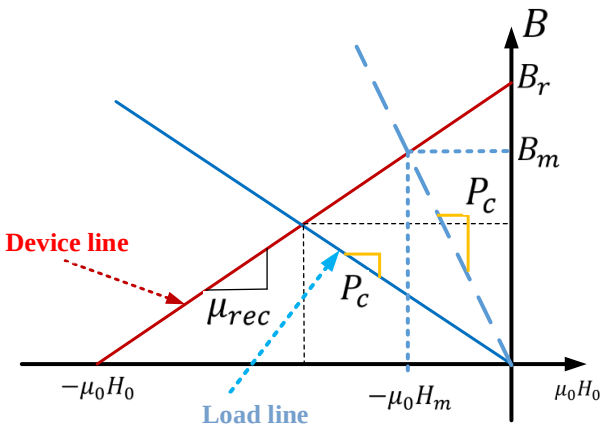

Figure 2 B-H curve of a permanent magnet material.

The straight-line demagnetization characteristic described by:

$$B_m = \mu_{rec}\mu_0 H_m + B_r \quad (13)$$

where B_r is the remanent flux density, B_m is the flux density in the magnet and H_m is the magnetizing force in the actual magnet. μ_{rec} is relative recovery permeability and μ_0 is the permeability on the air. There are two lines in Figure 2 called the device line and load line. The device line is defined as the theoretical demagnetization curve and the load line is the line through the origin to the working point. Therefore, the load line equation can be expressed as:

$$B_m = -\mu_0 \frac{d_m A_g}{g A_m} H_m = -P_c(\mu_0 H_m) \quad (14)$$

where Pc is called permanence coefficient, which is the slope of the load line and is equal to:

$$P_C = \frac{d_m A_g}{g A_m} \quad (15)$$

where A_g is air-gap area, and A_m is cross-sectional area providing the magnetic flux per pole. Thereby, can be defined as:

$$B_m = \alpha_m B_r \quad (16)$$

$$H_m = -(1-\alpha_m)H_c \quad (17)$$

where α_m is the pole arc coefficient of the permanent magnet, however, to avoid demagnetization and knee effect, it generally chooses a pole arc coefficient higher than 0.5 [19,21]. In this design, the pole arc coefficient to $\alpha_m = 0.75$ is selected. There are two parameters for the size of the permanent magnet of the outer rotor BLDCM, which are the thickness and axial length. In general motor design, the axial length of the permanent magnet is the same as the stack height of the stator core. In this paper, the surface mounted the outer rotor BLDCM is selected. The initial thickness of the permanent magnet can be approximated by the following formula.

$$l_m = \frac{\mu_{rec} g}{\frac{B_r}{B_g} - 1} \quad (18)$$

where μ_{rec} is the relative recovery permeability (1.085), g is the air gap length of the motor and $\frac{B_r}{B_g}$ is generally between 1.1 and 1.35. In this paper, the $\frac{B_r}{B_g}$ is chosen as 1.155.

A short air-gap length maximizes the flux for given thickness of magnet, but it also requires closer mechanical tolerances, increases cogging torque, and increases inductance. With these factors in mind, the range of air-gap length 0.5 – 1 mm is common in small motor. Therefore, the initial value of air-gap in this study is set to g = 0.5 mm. Thus, the initial l_m can be determined as: $l_m = 3.5$ mm

2.2.3 Dimensions of the Stator

The outer diameter of the stator, D_{so} can be determined as

$$D_{so} = D_{ro} - 2(l_m + g + b_{ry}) \quad (19)$$

$$D_{so} = 283 \text{ mm}$$

The outer diameter of the stator is 283 mm, then from $D^2_a L_a = 7208 \times 10^3$ mm^3, can be obtain L_a= 90 mm.

The total flux through the yoke is equal to the flux in the air gap via a half pole pitch [1]. Therefore, the core flux can be calculated as:

$$\Phi_{core} = \Phi_{gap,per\ half\ pitch} \quad (20)$$

$$\Phi_{core} \approx \frac{D_{so}}{N_r} L_{eff} B_{g,pk} \quad (21)$$

where L_{eff} is stator effective length and $B_{g,pk}$ is peak is air-gap flux density.

The stator yoke flux density can be obtained as:

$$B_{core} = \frac{l_{eff} B_{g,pk} D_{so}}{b_{sy} N_r L_a k_i} \quad (22)$$

where b_{sy} is stator yoke thickness, k_i is the factor considered in the insulation space between the laminations. The tooth pitch of the stator given by

$$\tau_s = \frac{\pi D_{so}}{N_s} = 37.045 \text{ mm} \quad (23)$$

The flux through one stator tooth is gained by integrating the air gap flux density over the

whole slot pitch.

$$\Phi_{tooth} = \tau_s L_{eff} B_{g,pk} \quad (24)$$

The relationship between the flux density of stator yoke, B_{core} and flux density of stator tooth, B_{tooth} can be obtained as:

$$\frac{B_{core}}{B_{tooth}} = \frac{T_w D_{so}}{\tau_s N_s b_{sy}} \quad (25)$$

Thereby, the yoke thickness can be expressed as:

$$b_{sy} = \frac{T_w D_{so} B_{tooth}}{\tau_s B_{core} N_s} \quad (26)$$

where T_w is tooth width. The empirical equations can be used to determine the stator slots' size [19-21]. Figure 3 shows the schematic structural view of the stator slots.

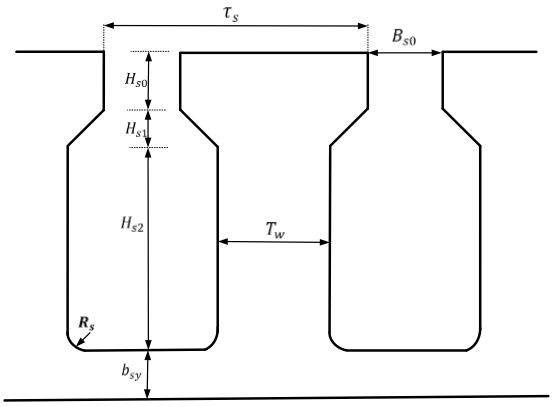

Figure-3 Stator slot dimensions.

The operating flux density of the machine depends on the stator tooth width T_w which is determined by:

$$0.4\tau_s \le T_W \le 0.6\tau_s \quad (27)$$

Thereby, it can be achieved by:

$T_W = 0.423\tau_s = 15.7$ mm

It is necessary that the stator slot depth H_{s2} should be large enough to increase the winding area, which is determined by:

$$1.5T_W \leq H_{s2} \leq 3T_W \quad (28)$$

In this paper, the H_{s2} is chosen as:

$H_{s2} = 1.59T_W = 25$ mm

Based on empirical equations the slot wedge height H_{s1}, slot opening height H_{s0}, and slot opening width B_{s0}, can be can be determined as

$$0.1b_s \leq H_{s1} \leq 0.5b_s \quad (29)$$

$$0.1b_s \leq H_{s0} \leq 0.5b_s \quad (30)$$

$$0.1b_s \leq B_{s0} \leq 0.5b_s \quad (31)$$

where $b_s = \tau_s - T_w$

In this paper, the initial value of H_{s1}, H_{s0} and B_{s0} are selected as:

$$H_{s1} = H_{s0} = 0.226b_s = 5 \text{ mm}$$

$$B_{s0} = 0.182b_s = 4 \text{ mm}$$

The winding's number of turns considerably affects the performance of the machine. The fact that it is given by this calculation is very significant, created on the basic of the phase winding voltage calculation. Thereby, the number of turns per coil N_c can be expressed as [19,20]

$$N_c = \frac{V_r C}{2\sqrt{2}\pi q f_e k_w T_W L_a B_{g,pk}} \quad (32)$$

where f_e is the fundamental electrical frequency, k_w is the winding factor, q is the number of phases, C is the number of parallel circuits of armature winding.

The mechanical speed, w_m is determined as:

$$w_m = \frac{\pi}{30} n_N \text{ rad/s} \quad (33)$$

Therefore, the phase frequency of the BLDC motor is given as

$$f_e = \frac{w_m}{2\pi} = \frac{n_N N_m}{60} = 116.667 \text{ Hz}$$

Assume the supply voltage V_r is 72 V, and flux density $B_{g,pk}$ is 0.9 T. Then, from above equation, the N_c of the proposed BLDCM design is obtained as 20 turns.

The slot fill factor F_{slot} indicates the ratio of the total cross-section area of the conductors to the total slot area, which includes the slot liners, slot separators, conductors and insulations. In this work, the slot filling factor is defined as the ratio of the cross-sectional area of the amount of material inside of a stator slot compared to the amount of total available space of slot.

$$F_{slot} = \frac{A_{wire} + A_{ins}}{A_{slot}} \quad (34)$$

where A_{slot} is the total cross-sectional area of slot, A_{ins} is total cross-sectional area of all insulating materials and A_{wire} is total area of wire. The initial design parameters of the proposed out-rotor BLDCM have been decided and are hereby given in Table 4.

Table-4 The initial design parameters of the specified 24/14 BLDCM

Parameter	Value
Number of stator teeth	24
Stator outer diameter [mm]	283
Stator yoke thickness [mm]	10.5
Stator inner diameter [mm]	192
Stator slot depth [mm]	35
Number of the turns per coil [Turns]	20
Number of rotor poles	14
Rotor outer diameter [mm]	313
Rotor outer diameter [mm]	313
Magnet thickness [mm]	3.5
Air-gap [mm]	0.5
Slot fill factor [%]	50.5

The finite element analysis (ANSYS-Maxwell) is utilized for investigating the performance of the initial design parameters. The values of efficiency, torque, cogging torque and slot fill factor at the initial design parameters are provided in Table 5. Table 5 shows that the performance of the initial design has the lower efficiencies and higher cogging torque. Therefore, the characteristic of the initial does not meet the requirements of the motor drive in the light electric vehicle.

Table -5 The 24/14 BLDCM performance at the initial design parameters.

Parameter	Value	Unit
Average input current	152.28	A
Voltage	72	V
Speed	501	Rpm
Power	10000	W
Efficiency	90.09	%
Torque	190. 8	N.m
Cogging torque	3.513	N.m
Torque ripple	11.35	%

3-Optimization Problem Definition of the BLDCM

The design optimization of a BLDCM starts form defining the optimization frame, which comprises the design of variables, objectives, and constraints. The aim of the design is to investigate and modify the motor geometry to enhance the average torque, maximum efficiency and minimize torque ripple.

The diagram of the prototype the 24/14 BLCDM is presented in Figure 1. However, for purposes of precisely defining the BLCDM dimensions, there are some design variables (DVs) to be considered, as shown in Figure 4.

From the previous Figure 4 there are 9 DVs to be investigated for the cross-section of the BLDCM. The next major parameters such as D_{so}, b_{sy}, g, l_m, T_w, b_{ry}, H_{so}, B_{so} and H_{s2} are optimized against the machine performance whilst fixing the number of turns per coil, N_c.

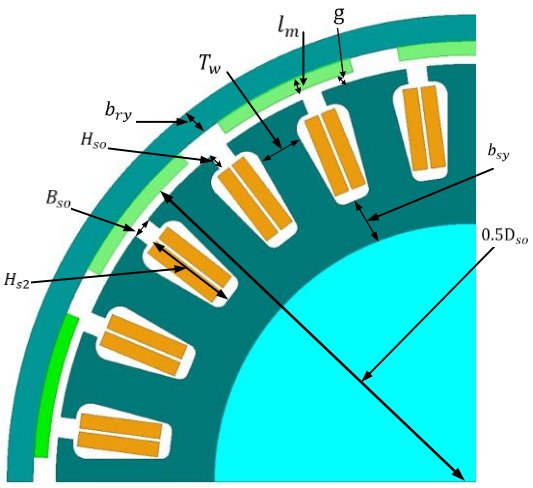

Figure 4 The dimension parameters of BLDCM.

Table 5 shows that the characteristic of the initial does not meet the requirements of the motor drive in for the light electric vehicle. Thus, the goals of the maximum average torque, maximum efficiency and the minimum torque ripple are selected for the objectives design optimization, in purpose to provide the design specifications of the BLDC motor. One of the challenges of multi-objective optimization is that the objectives usually conflict with each other, and no unique solution can be found [24,25]. An adopted strategy is to select single objective as the primary target and all the other objectives as constraints. The chosen principal goal is efficiency. The average torque must be meet the requirements of the motor drive in in the light electric vehicle. The torque ripple must be an in-limitation range of 7 % to 10 %. Therefore, the optimization model of a design problem with a single objective, 2 constraints and 9 design variables can be in the form:

$$\begin{cases} max & \{f_1(x_i)\} \\ s.t & \{g_1(x_i), g_2(x_i)\} \\ & \underline{x}_i \le x_i \le \overline{x}_i, \quad i=1,2,\ldots 9. \end{cases} \tag{35}$$

Where $f_1(x_i)$ is representing the objective function, which is the efficiency. The constraint functions $g_1(x_i)$ and $g_2(x_i)$ are the average torque and the torque ripple, respectively

The efficiency η, of a BLDCM is estimated considering only core and copper losses, as:

$$\eta = \frac{wT_{avg}}{wT_{avg} + P_{core} + P_{cu}} \tag{36}$$

Where w is the rotational speed, P_{core} is the core loss, and P_{cu} is the copper loss. The total copper loss of the BLDCM is determined as:

The specific core loss P_{core} in W/m3 can be expressed by theory of Bertotti equation [25-28]. The core loss is distributed into three items:

$$P_{core} = P_h + P_e + P_{ex} \quad (37)$$

where P_h, P_e and P_{ex} are hysteresis loss, eddy current loss and excess loss, respectively.

Further, the subject constraints on the optimization are:

The torque ripple T_r is defined as:

$$T_r = \frac{T_{max} - T_{min}}{T_{avg}} \quad (38)$$

where T_{max} and T_{min} are the maximum and minimum torque. The T_r is constrained as:

$$7 \leq T_r \leq 10\ \%$$

The average torque T_{avg}, should meet to specifically output torque of motor drive in the

$$190 \leq T_{avg} \leq 195 \text{ N.m} \quad (39)$$

The design optimization model mentioned above has a high dimension design space. In the conventional optimal design approaches, the constraints, and the objective function are carried out by utilizing an FEA simulation for every candidate design, which makes the method of searching the optimal solution to the BLDCM design problem computationally costly. This paper suggests using surrogate model to estimate the model on the procedures of screening the optimal solution, as to reduce computational cost.

This portion introduces an inclusive frame for MO optimization of the BLDC motor, as shown in Figure 5. The planned structure starts through the optimization model Equation (35) and is continued by four major portions which are illustrated with the subsequent parts: DOE, SA, construction of the SMs, and the SPO based SMs.

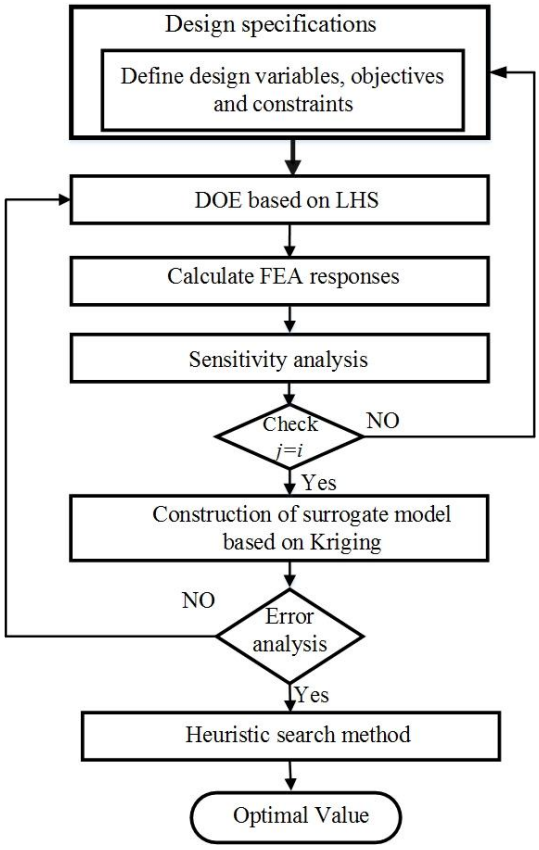

Figure-5 Flow chart of the proposed design optimization

3.1 Design of Experiment

DoE is targeted to utilize the smaller number of generated sampling points of the design spaces for compiling the largest amount of information [26-28]. It is developed to minimize the bias and random error in the sampling generation and to achieve the SMs more precise. The LHS [29] is a model category of modern DoE technology extensively used in computations. The LHS has two advantage characteristics among the others categories of the modern DOE. (1) The evaluation of the mean value can be provided by LHS, it is much more precise. (2) It is not limited by the number of the sampling points. Thus, it would permit the employee to control the intricacy and the times of calculation for generating the sampling. The generation of sampling points is established on two rules. (a) It is separate and randomly chosen. (b) In every part, only one sample is allowed. The analytical equation for carrying out LHS sampling as

$$x_j^{(i)} = \frac{\pi_j^{(i)} + U_j^{(i)}}{k} \quad (40)$$

for $1 \le j \le n$ and $1 \le i \le k$, where k is the number of samples, n is the number of design variables, U is a uniform value between [0, 1], and π is an independent random permutation of the sequence of integer 0 , 1, , k – 1. Subscript j denotes the dimension number and superscript i denotes the sample number. As a development through the unconstrained applied sampling technique, LHS can be used to design variables that have an atypical probability classification, additionally correlations between the variables [29]. Consequently, it is chosen as the distinguished DOE method of this part.

3.2 Sensitivity Analysis

SA is performed to reduce the number of IDVs. SA can also provide essential prudence on how every design variable impacts the apparatus characteristics. In this part, the SA method is applied to calculable to measure the sensitivities of the apparatus performance to every design variable [30]. The DoE based on LHS is carried out in an FEA simulation to compute the machine performance, thus the variance is estimated based on the FEA simulation results. The SA is calculated by the sensitivity guide that considers the proportional significance of the variable only and is explained as follows [30, 31].

$$S_{xi} = \frac{V_{xi}(E_{x\sim i}(\boldsymbol{y}|x_i))}{V(\boldsymbol{y})} \quad (41)$$

where $E_{x\sim i}(\boldsymbol{y}|x_i)$ is the mean of $\boldsymbol{y}$ taken through $x\sim i$ (all variables except for x_i) when x_i is constant, $V_{xi}E_{x\sim i}(\boldsymbol{y}|x_i)$ is the conditional variance of $E_{x\sim i}(\boldsymbol{y}|x_i)$, and $V(\boldsymbol{y})$ is the variance of $\boldsymbol{y}$. The model of SA comprises the input x_i and output $\boldsymbol{y}$. The input is design variables, x_i , as [D_{so}, b_{sy}, g, l_m, T_w, b_{ry}, H_{so}, B_{so}, H_{s2}]. The output y, includes η , T_r and T_{avg}. The sensitivity of significant design variable x_i on output $\boldsymbol{y}$ must satisfy the following Equation (42) [32].

$$S_{xi} \ge 0.2 \quad (42)$$

First, the sampling plan is generated for x_i using the LHS realization of 100 samples, which is carried out via MATLAB Software. Therefore, each sample point is run in the FEA, which is carried out through ANSYS-Maxwell to obtain the output $\boldsymbol{y}$. Then, we apply thex_i, and $\boldsymbol{y}$, in Equation (41). A greater sensitivity indicator marks a higher impact to $\boldsymbol{y}$ by x_i. Therefore, the SA of the three BLDCM performance η , T_r and T_{avg} , to the 9 DVs are evaluated, and the outcomes are shown in Figure 6. Equation (42) and Figure 6 show that [D_{so}, b_{sy}, g, l_m, T_w, b_{ry}, H_{s2}] are significant DVs for the BLDCM optimization. These design variables are relevant to magnetic resistance and have a lot of impact on flux linkage-current characteristics of the BLDCM. The influences of the other DVs [H_{so}, B_{so}] have insignificant influences on efficiency and average torque. Therefore, the number of DVs in the following design optimization process is reduced from 9 to 7 DVs.

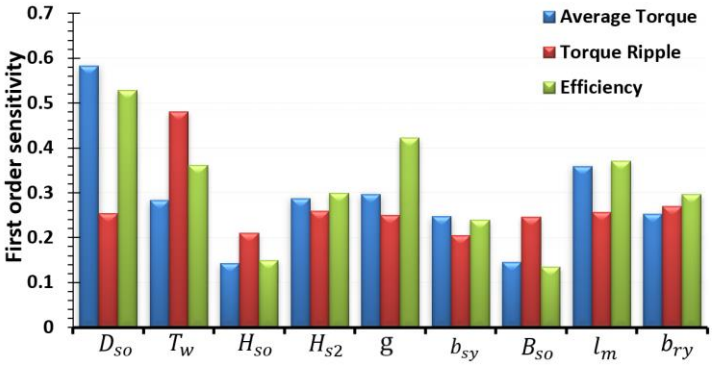

Figure-6 Sensitivity indices of efficiency, average torque and torque ripple to the 9 design variables for the BLDCM

3.3 Construction of Surrogate Models

After the SA, the SMs are created by implementing the DoE and FEA. The accuracy of SMs effectively depends on both the type of the SMs and the DoE. Two types of SMs are generally considered: parametric and non-parametric approaches. Compromise approaches called the Kriging model have become popular in recent years [33,34]. Kriging model in multi-dimensions, which takes the global estimation model for a response $y(t)$ is described as:

$$y(t) = \beta + z(t) \quad (43)$$

where $z(t)$ is the fundamental function introduced by Gaussian distribution whose variance and mean are σ^2 and 0, respectively; and β is the constant.

Several kinds of literature have been considerations to contrast the precision for types of the SMs; the Kriging technique is contemplated to be reasonably precise for predicting the complex systems [35-37]. consequently, the Kriging technique is utilized in the SMs of this part.

3.4 Heuristic Search Method

Following the creation Kriging technique, the optimization process should be utilized to locate the local best performance. The optimization of electrical machines is a

multi-variable and multimodal problem [14,15,38]. At current, two major types of evolutionary optimization algorithms are commonly adopted by PSO and GA. PSO is a stochastic algorithm developed for optimizing continuous, nonlinear, constrained or non-constrained, non-differentiable multi-objective functions. The process of PSO progressively modifications the velocity of every particle of, it is the personal best (pbest) and the global best (gbest) location each time. Figure 7 shows the update of a particle position X_j^k in the PSO using a combination of the old velocity V_j^k, the direction to the local best position P_j^k and the direction to the global best position P_g^k. The new velocity and location of particles are obtained as:

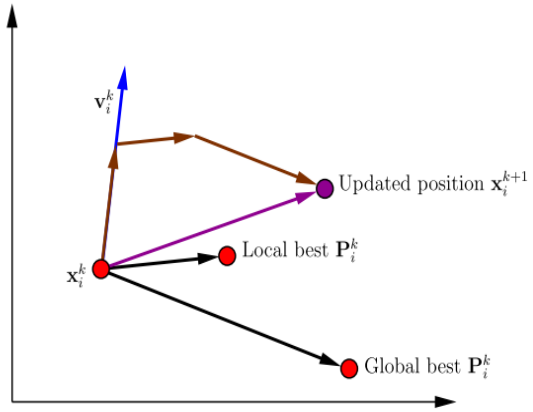

Figure-7 Procedure of particle swarm optimization [38].

$$V_j^{(k+1)} = V_j^k + C_1\varphi_1(P_j^k - X_j^k) + C_2\varphi_2(P_g^k - X_j^k)$$

$$X_j^{(k+1)} = X_j^k + V_j^{(k+1)}$$

where V_j^k and X_j^k represent the velocity and position of the jth particles in iteration k; P_j^k is the pbest of particle j in iteration k, and P_g^k is the gbest of all the particles in iteration k. C_1 and C_2 are the weight ratios; φ_1 and φ_2 are uniformly distributed to random numbers between 0 and 1.

The first term explains the inertia, which causes the particles to transfer in the same orientation. The second and third terms ensure the particles follow the gbest and pbest. The PSO is widely used in various fields and applied to different optimization problems [19,20,39,40]. Among the other calculation intelligence-based methods, PSO has its benefits including simply carrying out, having a more effective memory capacity, and being more advantages in maintaining the diversity of the swarm [41-43]. Hence, PSO is chosen to be employed in this work. The number of particles j in this work is 7 DVs such as [D_{so}, b_{sy}, g, l_m, T_w, b_{ry}, H_{s2}]

4. Numerical results and analysis

The optimization model of design problem has a single objective, 2 constraints and 7 design variables. The optimization function of the out-rotor BLDCM is defined in Table 6 as:

Table-6 The optimization function of the out-rotor BLDCM

The objectives	The constraints	The design variables
Maximize η	$190 \le T_{avg} \le 195$ [N.m]	$275 \le D_{so} \le 283$ [mm]
		$10.5 \le b_{sy} \le 12.8$ [mm]
		$0.35 \le g \le 0.55$ [mm]
		$3.25 \le l_m \le 3.7$ [mm]
		$15.5 \le T_w \le 16.5$ [mm]
		$10.8 \le b_{ry} \le 11.5$ [mm]
	$7 \le T_r \le 10$ [%]	$24 \le H_{s2} \le 25$ [mm]

This optimization is designed to identify the best performance of the BLDCM, i.e., which maximizes efficiency. According to the LHS for the BLDCM optimization with 7 design variables D_{so}, b_{sy}, g, l_m, T_w, b_{ry} and H_{s2} with a total of 100 sampling points have been generated, which is achieved via Matlab software. Then each sampling point is run in the FEA to obtain the results used to construct the initial surrogate model. Once the simulation results have been calculated, the efficiency average torque and torque ripple contour of the BLDCM optimization function with independent variables D_{so}, b_{sy}, g, l_m, T_w, b_{ry} and H_{s2} are presented in Figures 8, 9 and 10.

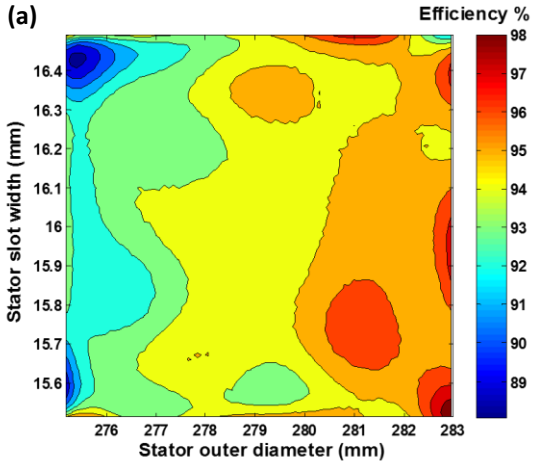

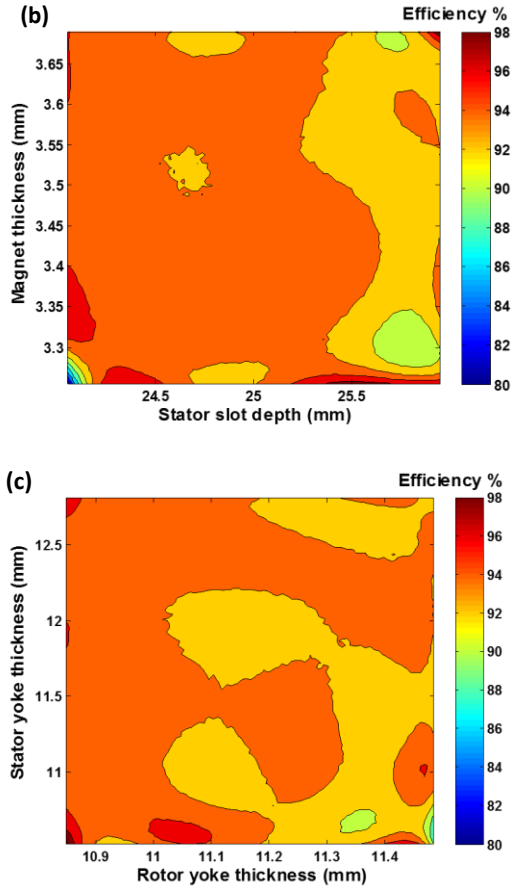

Figure-8 Preliminary surrogate results of efficiency contour (a) Stator slot width and stator outer diameter, (b) magnet thickness and stator slot depth and (c) stator yoke and rotor yoke.

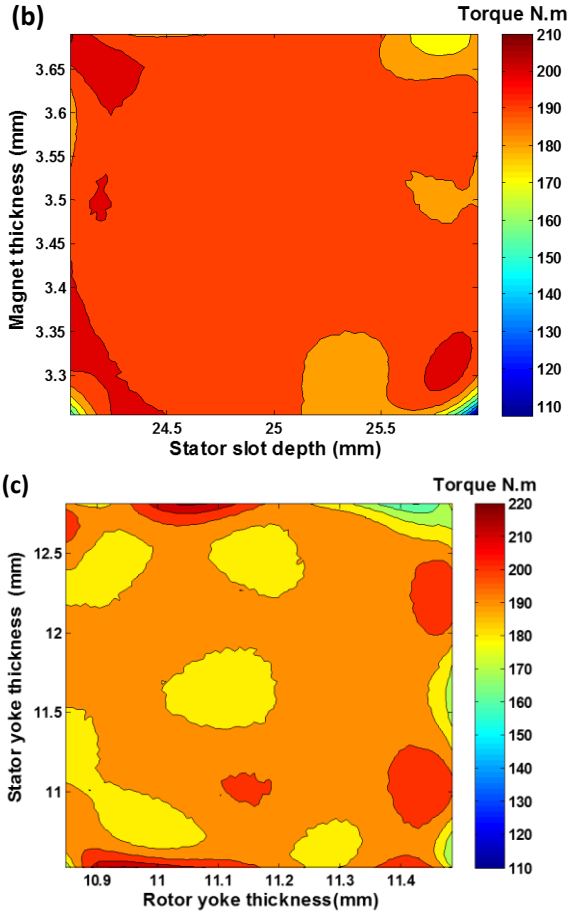

Figure-9 Preliminary surrogate results of average torque contour (a) Stator slot width and stator outer diameter, (b) magnet thickness and stator slot depth and (c) stator yoke and rotor yoke.

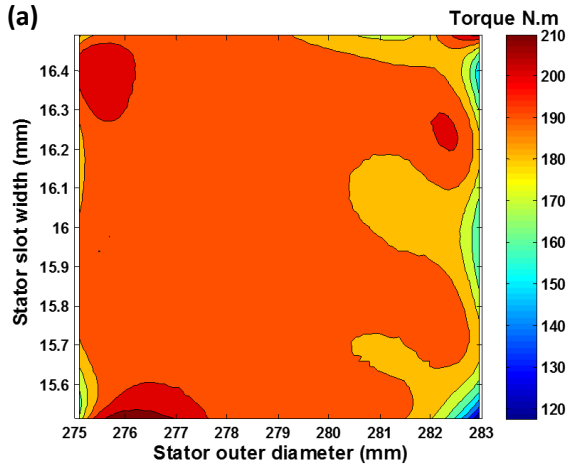

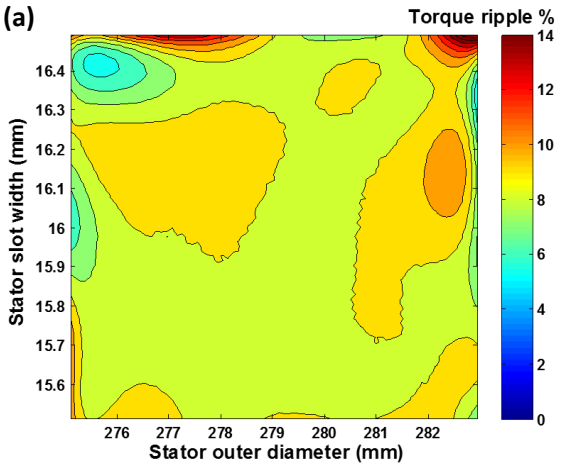

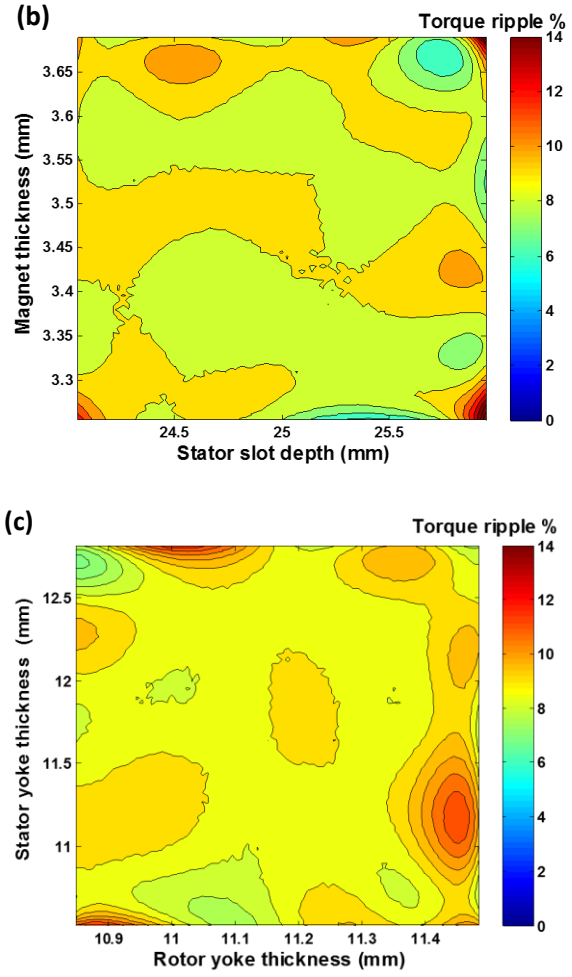

Figure-10 Preliminary surrogate results of torque ripple contour (a) Stator slot width and stator outer diameter, (b) magnet thickness and stator slot depth and (c) stator yoke and rotor yoke.

Three-dimensional distributions of the efficiency and average torque versus independent variables D_{so}, T_w, l_m and H_{s2} are presented in Figures 11 and 12.

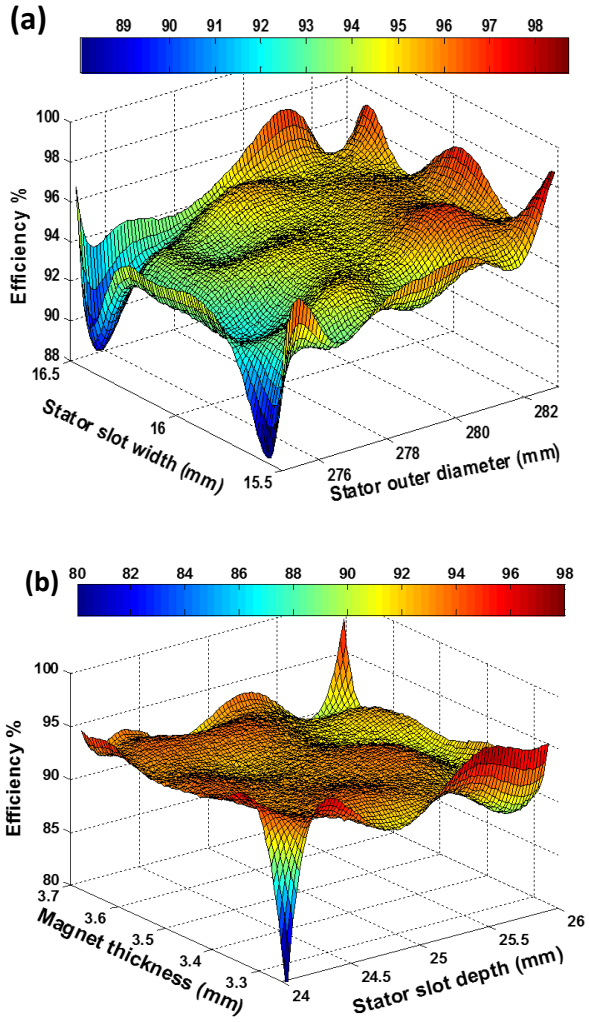

Figure -11 Three-dimensional distributions of the Efficiency (a) Stator slot width and stator outer diameter and (b) magnet thickness and stator slot depth.

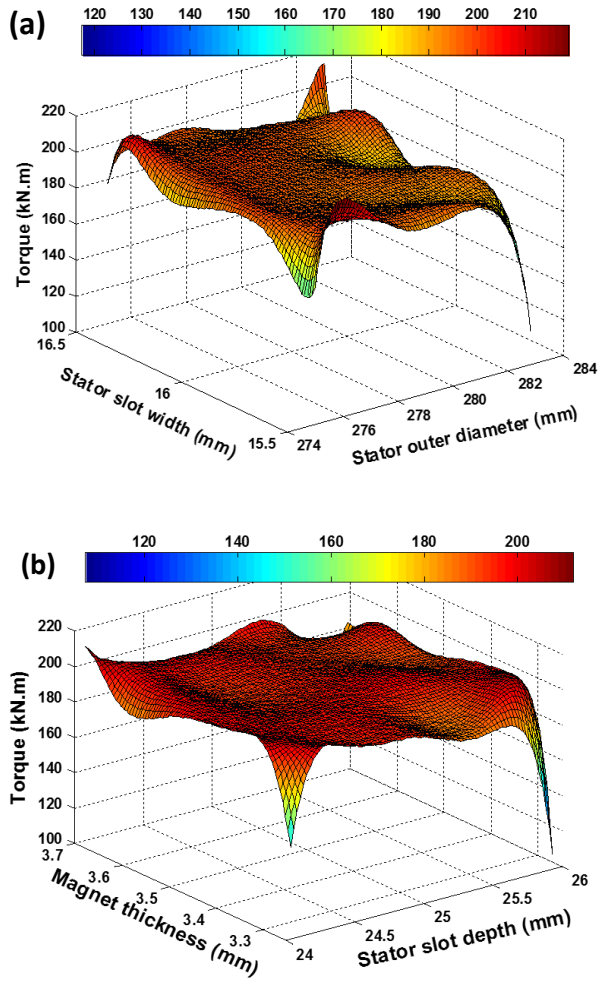

Figure-12 Three-dimensional distributions of average torque (a) Stator slot width and stator outer diameter and (b) magnet thickness and stator slot depth.

Currently, the surrogate model of the BLDCM with 7 variables has already been constructed, which can be searched for the local best point. As shown in Figures 8-12 the surrogate model indicates that the efficiency, average torque and torque ripple are quite nonlinear and distributed unevenly around the entire design region.

Therefore, the PSO search algorithm is adopted for optimization. The optimization process utilizes PSO is carried out via Matlab software. The optimal final best point [D_{so}, b_{sy}, g, l_m, T_w, b_{ry}, H_{s2}] is set at [281.5, 11.45, 0.44, 3.36, 15.9, 11.2, 25.5]. Thus, the other dimensions of the motor can be determined through Equations mentioned in section 3. The geometrical dimensions of the final design of the specified BLDCM are detailed in Table 7.

Table-7 The geometrical dimensions of the optimal design of the specified BLDCM.

Parameter	Value
Number of stator teeth	24
Stator outer diameter, D_{so} [mm]	281.5
Stator yoke thickness, b_{sy} [mm]	11.45
Stator inner diameter, D_{si} [mm]	187.5
Stator slot depth, H_{s2} [mm]	25.5
Stator slot width, T_w [mm]	15.9
Number of the turns per coil [Turns]	20
Number of rotor poles	14
Rotor outer diameter, D_{ro} [mm]	311.5
Rotor yoke thickness, b_{ry} [mm]	11.20
Magnet thickness, l_m [mm]	3.36
Air-gap, g [mm]	0.44
slot opening width, B_{s0} [mm]	4
Slot fill factor [%]	51.52

The finite element analysis (ANSYS-Maxwell) is utilized for investigating the performance of the optimal design parameters. The values of efficiency, torque, cogging torque and slot fill factor at the initial design parameters are provided in Table 8. Table 8 shows that the performance of the initial design has higher efficiencies and lower cogging torque. Therefore, the characteristic of the optimal design meets the requirements of the motor drive in the light electric vehicle.

Table-8 The 24/14 BLDCM performance at the optimal design parameters.

Parameter	Value	Unit
Average input current	145.82	A
Voltage	72	V
Speed	500.5	rpm
Power	10000	W
Total loss	498.5	W
Slot fill factor	51.52	%
Efficiency	95.25	%
Torque	190.04	N.m
Cogging torque	1.56	N.m
Torque ripple	8.15	%

The results of optimization based on the surrogate models are confirmed by FEA (ANSYS Maxwell) simulation. To substantiate the precision of the surrogate models compares to FEA, several test points (generated by LHS) are also simulated with the optimized point. The validation results are presented in Table 9. As indicated in Table 8, the accuracy of the surrogate model is validated by FEA simulation. Table 9 shows that, the point [281.5, 11.45, 0.44, 3.36, 15.9, 11.2, 25.5] is the local best point of the BLDCM. It is because at this point, the maximum value of efficiency and minimum value of torque ripple are obtained, as well the required torque of the motor is acquired. Table 9 A comparison of accuracy between FEA and SM results. The FEA (ANSYS-Maxwell) is utilized for investigating the performance of BLDCM. Figure 13 shows the efficiency versus speed of the BLDCM. The maximum efficiency 95.5% is obtained at speed 500 rpm.

Moreover, the electromagnetic torque and cogging torque of the BLDCM at the optimal final point is specified as functions of the rotor position, as shown in Figures 14 and Figure 15. Average of the torque is obtained as 190 Nm. Figure 15 shows the cogging torque generated due to the different magnetic resistance of difference path generated by the pole-pitch structure of the proposed BLDCM. The maximum cogging torque is 1.98 N and the average value is 1.56 N.m.

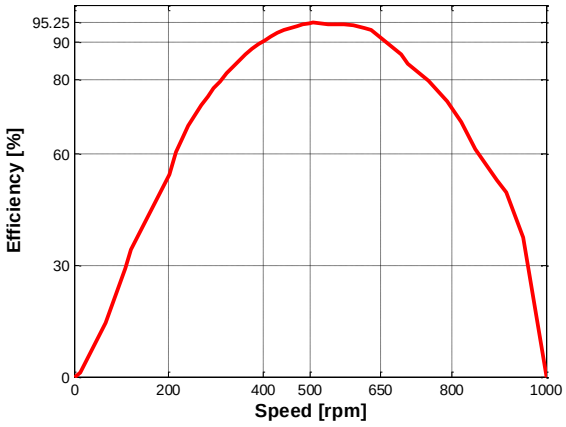

Figure 13 Efficiency versus speed

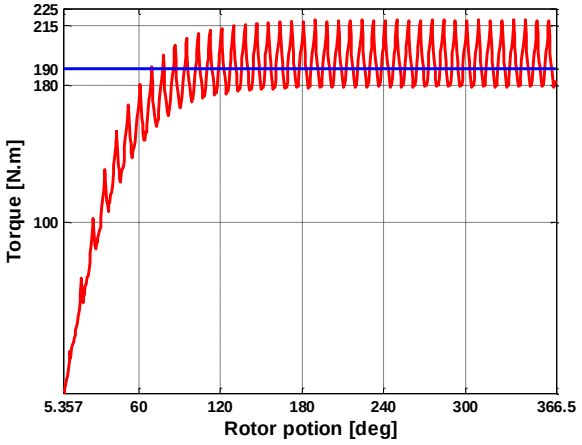

Figure-14 Averages torque versus rotor position

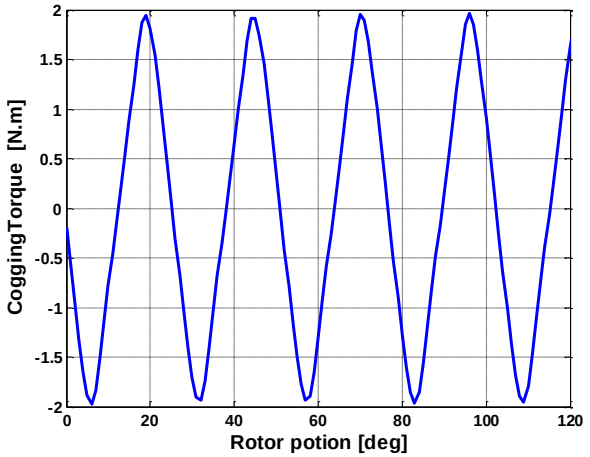

Figure-15 Cogging torque versus rotor position

Table 9 A comparison of accuracy between FEA and SM results

Item	$[D_{so}, b_{sy}, g, l_m, T_w, b_{ry}, H_{s2}]$	FEA η%	SMs η%	Error %	FEA Tavg	SMs Tavg	Error N.m	FEA Tr%	SMs Tr%	Error %
Test_1	[282;12;0.51;3.60;16;11.21; 25.82]	94.35	94.25	0.1	191.71	191.02	0.69	9.41	9.37	0.04
Test_2	[278;11.30;0.52;3.54;16.3;11.1;24.7]	93.32	93.40	-0.08	190.27	190.35	-.18	8.21	8.23	-0.02
Test_3	[283;10.84;0.5;3.43;16.1;11.43;25.91]	94.73	94.85	-0.12	180.91	180.34	0.57	10.1	10.05	0.05
Test_4	[280.1;11.5;0.53; 3.41;15.7;11.3;24.52]	93.87	93.95	-0.08	190.96	190.25	0.71	8.24	8.21	0.03
Test_5	[277.5;11.32;0.54;3.62;16.15;10.95;25.51]	93.22	93.15	0.07	189.95	189.52	0.43	9.72	9.65	0.07
Best	[281.8;11.45;0.44;3.36;15.8;11.2; 25.5]	95.42	95.46	-0.04	190.64	190.04	0.6	8.11	8.15	-0.04

A finite element simulation was performed here at a speed of 500.5 rpm and a load of 190 Nm. The winding current curve obtained by the simulation is shown in Figure 16.

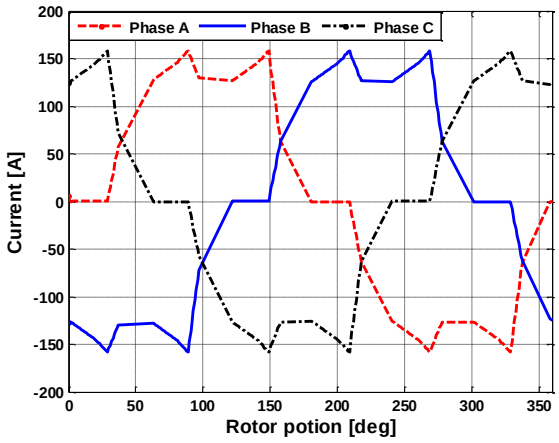

Figure-16 Load three-phase winding current

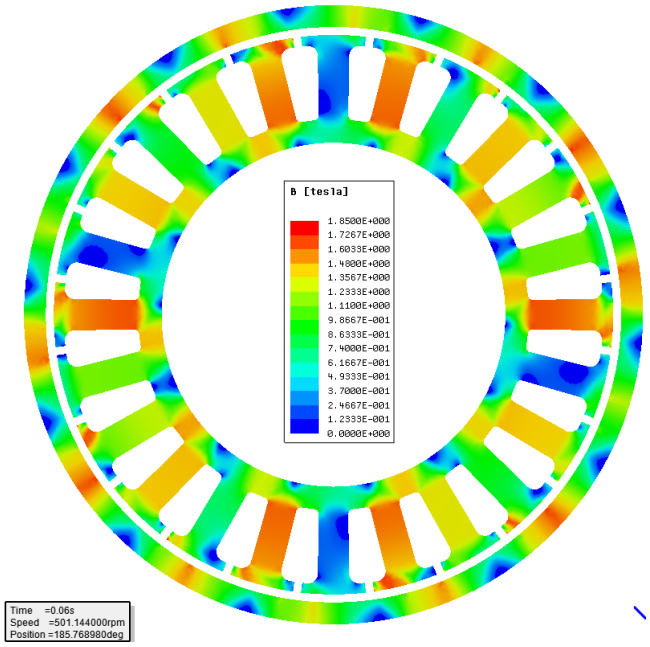

Figure-17 The distributions of the flux density

The flux density and flux line distribution in the motor at rated speed 501 rpm and the optimal point can be seen in Figure 17 and Figure 18. The average flux density of the stator and rotor poles about 1.7 T, thus, it can be confirmed the design constraint.

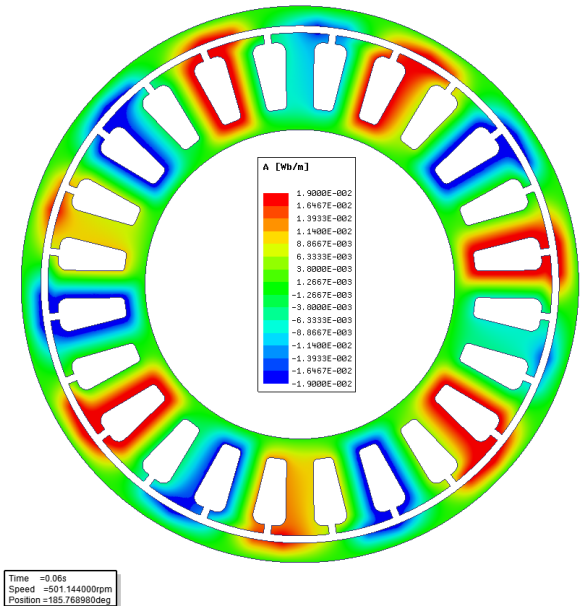

Figure-18 The distributions of the flux line

5. Conclusion

The paper has presented the design and optimization of the BLDC motor for light electrical vehicle. Design of experiment techniques are developed, whilst one of these-the LHS plan is selected to generate the random and uniform sampling distributions. The optimization based on the SMs of the BLDC motor is started with 9 independent design items. Based on the sensitivity analysis, the number of design elements is reduced to 7 variables. Methods of construction of the SMs are investigated; the Kriging model is chosen to construct the SMs due to its higher precision. Based on the SMs built, an optimization algorithm is used to find the best location, and in this work, the PSO algorithm is adopted. The optimization results have been successfully validated by using the FEA. Moreover, the computational cost of the proposed technique of optimizations based on SMs is lower than the conventional optimal design techniques based on an FEA, without sacrificing the precision of the BLDC motor design.

REFERENCES

[1] Noor, F.; Padmanaban, S.; Mihet, L.; Mollah, M.; Hossain, E. A comprehensive study of key electric vehicle (EV) components,technologies, challenges, impacts, and future direction of development. Energies 2017, 10, 1217-.

[2] De, J.; Bernhoff H.; Ekergård, B.; Eriksson, S.; Ferhatovic, S.; Waters R.; Leijon, M. Electrical motor drivelines in commercial all-electric vehicles: A review. IEEE Transactions on vehicular technology, 2011, 61, 475–484.

[3] Booker, A.; Dennis, J.; Frank, P.; Serafini, D.; Torczon, V. Optimization using surrogate objectives on a helicopter test example. Birkhauser, Boston, 1998; ISBN 978-1-4612-1780-0.

[4] Zheng, T. Improved winding design of a double fed induction generator (DFIG) wind turbine using surrogate optimization algorithm. Ph.D. Thesis, Newcastle University, Edinburgh, Scotland. 2016.

[5] Wang, G Gary.; Seong K. Adaptive response surface method using inherited latin hypercube design points. J. Mech. Des.2003, 125, 210-220.

[6] Duan, Y.; Ionel, M. A review of recent developments in electrical machine design optimization methods with a permanent-magnet synchronous motor benchmark study. IEEE Trans.Ind. Electron. 2013, 49, 1268-1275.

[7] Song, X.; Lv, L.; Li, J.; Sun, W.; Zhang, J. An advanced and robust ensemble surrogate model: extended adaptive hybrid functions. J. Mech. Des. 2018, 4.

[8] [Song, X.; Zhang, J.; Kang, S.; Ma, M.; Ji, B.; Cao, W.; Pickert, V. Surrogate-based analysis and optimization for the design of heat sinks with jet impingement. IEEE Trans. Ind. Comp. Pack. Manuf. Tech. 2013, 4, 429-434.

[9] Queipo, N,; Haftka, R.; Shyy, W.; Goel, T.; Vaidyanathan, R.; Tucker, P. Surrogate- based analysis and optimization. Prog. aero. sci. 2005, 41, 1-28.

[10] Yang, N.; Cao, W.; Liu, Z.; Tan, Z.; Zhang, Y.; Yu, S.; Morrow, J. Novel asymmetrical rotor design for easy assembly and repair of rotor windings in synchronous generators. In Proceedings of the 2015 IEEE International Magnetics Conference (INTERMAG), Beijing, China, 11-15 May 2015; pp. 1-1.

[11] Yuan T.; Yang N.; Zhang W.; Cao W.; Xing N.; Tan Z.; Li G. Improved Synchronous Machine Rotor Design for the Easy Assembly of Excitation Coils Based on Surrogate Optimization. Energies. 2018, 5, 1311.

[12] Kennedy, J.; Eberhart, R. Particle swarm optimization. Proceedings of ICNN'95 International Conference on Neural Networks, 1995; pp. 1942-1948.

[13] Santner, T.; Williams, B.; Notz, W.; Williams, B. The design and analysis of computer experiments. New York: Springer, 2003.

[14] Koehler, J.Owen, A. Computer experiments. Handb. stat. 1996, 13, 261-308.

[15] McKay M.; D. Beckman; Richard J.; Conover W. Comparison of three methods for selecting values of input variables in the analysis of output from a computer code. Techn. 1979, 21, 239-245.

[16] Hu Y.;, Song Hui. Electric vehicles. eople's Communications Press, Beijing, China, 2006.

[17] Song Youchuan. Research on Design method of Electric Wheels for New Generation Electric Vehicles. Ph.D. Thesis, Wuhan: Huazhong University of Science and Technology. 2004.

[18] Chen, Q.; Liao, C.; Ouyang, A.; Li, X.; Xiao, Q. Research and development of inwheel motor driving technology for electric vehicles. Int. J. Elec. Hyb. Veh. 2016, 8, 242-254

[19] SONG Z. The research and development of the in-wheel-motor for light and low speed electric vehicle. Ph.D. Zhejiang University. 2015.

[20] Miller, T. Permanent magnet and reluctance motor drives. Oxford, UK: Oxford Science Publications, 1989.

[21] Hanselman, Duane C. Brushless permanent magnet motor design. The Writers' Collective, 2003.

[22] Handershot, R. Miller, E. Design of Brush-less Permanent Magnet Motors. Oxford, UK: Oxford Science Publications, 1994.

[23] D. Ishak; Z. Zhu; D. Howe. Comparison of PM brushless motors, with either all or alternative wound teeth. IEEE Trans. on Energy Conversion. 2006, 21, 95-103.

[24] Tudorache, T.; Popescu, M. Optimal design solutions for permanent magnet synchronous machines. Adv. Elect. Comp. Eng. 2011, 11, 77-82.

[25] Duan Y.; Ionel M. A review of recent developments in electrical machine design optimization methods with a permanent-magnet synchronous motor benchmark study. IEEE Trans. Ind. Appls. 2013, 49,1268-1275.

[26] Awad, M.; Khanna, R. Efficient learning machines: theories, concepts, and applications for engineers and system designers.Apress, 2015.

[27] McKay, M.; Beckman, R.; Conover, J. Comparison of three methods for selecting values of input variables in the analysis of output from a computer code. Technometrics. 1979, 21, 239-245.

[28] Giunta, A.; Wojtkiewicz, S.; Eldred, M. Overview of modern design of experiments methods for computational simulations. In Proceedings of the 41st Aerospace Sciences Meeting and Exhibit, USA, 2003; pp. 649.

[29] Saltelli, A.; Ratto, M.; Andres, T.; Campolongo, F.; Cariboni, J.; Gatelli, D.; Saisana, M.; Tarantola, S. Global sensitivity analysis: the primer. John Wiley & Sons, 2008.

[30] Homma, T.; Saltelli, A. Importance measures in global sensitivity analysis of nonlinear models. Rel. Eng. & Sys. Saf. 1996, 52, 1-17.

[31] Sasena Michael James. Flexibility and efficiency enhancements for constrained global design optimization with kriging approximations. Ph.D. University of Michigan,USA. 2002.

[32] Duvigneau, Praveen C. Radial basis functions and kriging metamodels for aerodynamic optimization. INRIA Document. 1996, 52, 26-30

[33] Costa, J.; Pronzato, L.; Thierry, Eric. A comparison between Kriging and radial basis function networks for nonlinear prediction. NSIP. 1999, 726-730.

[34] Li, X.; Yao, Xin. Cooperatively coevolving particle swarms for large scale optimization. IEEE Trans. Evol. Comp. 2011, 16 210-224.

[35] Qu, Bo-Y.; Ponnuthurai N.; Liang, Jane. Differential evolution with neighborhood mutation for multimodal optimization. IEEE Trans. Evol. Comp. 2012, 16 601-614.

[36] I., Muhammad; Hashima, R.; Khalidb, N. An overview of particle swarm optimization variants. Procedia Engineering. 2013, 53 491-496.

[37] Van den B.; Engelbrecht, A. A study of particle swarm optimization particle trajectories. Inf. sci. 2006, 176, 937-971.

[38] Zhang, P.; Ionel, D.; Demerdash, N. Morphing parametric modeling and design optimization of spoke and V-type permanent magnet machines by combined design of experiments and differential evolution algorithms. In Proceedings of 2013 IEEE Energy Conversion Congress and Exposition, Denver, Colorado, USA, 15-19 September 2013; pp. 5056-5063.

[39] Hassan, R.; Cohanim, B.; De Weck, O.; Venter, G. A comparison of particle swarm optimization and the genetic algorithm. In Proceedings of 46th AIAA/ASME/ASCE/AHS/ASC structures, structural dynamics and materials conference, Austin, Texas, USA, 21 April 2005; pp. 1897

BIOGRAPHIES

Almarri Jaber received his B.S in Electrical Engineering, Dalian University of Technology (DLUT), China. His current research includes electric machines and drives, power electronics.